Structures of Binary $C_{60}-C_{84}$ Fullerene Clusters†

G. J. Bubnis and H. R. Mayne*

Department of Chemistry, University of New Hampshire, Durham, New Hampshire 03824

Received: December 21, 2008; Revised Manuscript Received: February 20, 2009

A systematic study of the potential energy global minimum (GM) structures of model binary fullerene clusters of compositions $(C_{60})_n(C_{84})_{N-n}$, $N \leq 24$ has been carried out using the basin-hopping method. The stiff Girifalco pair potential is used. We report a novel GM geometry for $(C_{84})_{13}$ with D_5 geometry. To the best of our knowledge, this is the first reported homogeneous 13-particle cluster whose potential is pairwise additive that has this structure. For homogeneous fullerene clusters larger than $N = 13$, the dominant packing motif is decahedral. By contrast, for the binary clusters studied, polyicosahedral structures are observed for a broad range of cluster sizes and compositions. It is pointed out how the favorable size ratio reduces strain to produce these packing motifs. For $N = 23$ and $N = 24$, we observe a reduced strain "stacked" polyicosahedral motif between the compact polyicosahedral and decahedral stability regions. Mackay-icosahedron based GMs were found for clusters $(C_{60})_1$ $(C_{84})_{N-1}$, $N > 18$.

I. Introduction

Since their discovery in 1985, fullerenes[1] have been recognized as a rich potential area for research. Thin films of fullerene derivatives have a wide range of photochemical and electrical properties.[2−4] Among many other technological possibilities, they have considerable potential applications in molecular electronics.[5]

There is also considerable interest in using functionalized fullerenes to generate self-assembled supramolecular structures both on surfaces and in solution phases.[2−4,6−9] Such structures may have important technological applications in creating nanoscale templates.[10] The full understanding of self-assembly using noncovalent interactions requires a knowledge of the intermolecular interaction between species, together with a comprehension of how these intermolecular interactions influence the possible growth sequence and structure of supramolecular assemblies. The detailed study of assemblies whose structure is dominated by noncovalent intermolecular interactions—such as atomic and molecular clusters and biomolecules—is a rich one and has been the subject of considerable current research activity.[11−14]

If theory or modeling are to guide experiment in this field, greater understanding of the details of the potential energy surface and the role this surface plays in kinetics and thermodynamics is desirable. A good first step is to address the role played by the potential energy in the formation and stability of gas phase clusters. Gas-phase clusters of C_{60} fullerene molecules have been investigated in considerable detail both experimentally and theoretically.[11,15−20] Recently, it has been shown that the pairwise additive approximation is not sufficiently accurate to agree with all the available experimental data.[17] However, many of the properties of C_{60} fullerene clusters can be at least qualitatively understood by assuming they interact through a pairwise-additive potential in which each is treated as if it were a pseudoatom. In particular, we use the Girifalco pair potential[19,21] which has been shown to reproduce many of the details of the fullerene cluster growth sequence. We will use this approximation here to facilitate the connection of our findings with the extensive theoretical literature that has used the same potential.

Understanding the growth sequence and structure of homogeneous gas phase clusters has been an active area of research in recent years.[11,20,22−28] With the recent availability of efficient search algorithms to locate the cluster geometry which is the global minimum (GM) of the potential energy surface,[11,14,27−31] connections between the details of the potential energy function and the cluster geometry are now generally well understood. In particular, there is a large body of knowledge for pairwise additive potentials. Shown in the lower part of Figure 1 are the fullerene−fullerene pair potentials used here.

A particularly useful model pair potential function is the Morse potential:

$$\frac{V_M(r)}{\varepsilon} = e^{\rho(1-r/r_e)}(e^{\rho(1-r/r_e)} - 2) \qquad (1)$$

The three parameters of the Morse potential are: the equilibrium separation, r_e; the potential energy well depth, $V_M(r_e) = \epsilon$; and the dimensionless range parameter, ρ. The independent variable is the dimensionless variable r/r_e, and the potential energy is in units of ϵ. Plotting in these scaled units allows the qualitative properties of potential functions to be readily compared, even if they differ significantly quantitatively. Pair potentials can be locally fit to a Morse function about the minimum of the potential curve. Although the fit to the full potential is not perfect globally, this has proved very useful in monitoring how properties change with the range parameter.[11,22,23]

In the upper part of Figure 1 we show the Girifalco potential for $C_{60}-C_{60}$. Also shown is a Morse fit to this potenetial, and the LJ potential which reproduces only the ϵ and the r_e. As can be seen, the LJ is a "soft" potential, with $V(r > r_e)$ increasing more slowly as a function of r than the "stiff" Girifalco potential. The stiffness parameter for the Lennard−Jones potential is found to be $\rho = 6.0$,[22,23,25] compared with $\rho = 13.6$ for the Morse. It should be noted that the long-range Girifalco potential is somewhat more attractive than the corresponding Morse potential.

* To whom correspondence should be addressed. E-mail: howard.mayne@unh.edu.

† Part of the "George C. Schatz Festschrift".

10.1021/jp811290h CCC: $40.75
Published on Web 03/20/2009

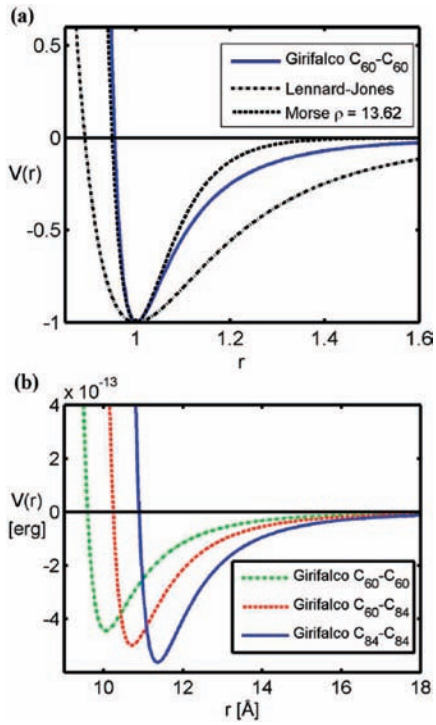

Figure 1. (a) Comparison of pairwise-additive potentials in reduced units of distance and energy. The Morse (ρ =13.62) potential shown has the same curvature as the Girifalco $C_{60}-C_{60}$ potential at the minimum. The Lennard-Jones potential shown has the same well depth. (b) Comparison of Girifalco fullerene-fullerene potentials used in this study.

From eq 1 and the above discussion, it can be seen that the range parameter will play a role in determining cluster structure.[11,22,23] For soft potentials nearest-neighbor (NN) interactions at separations not very different from r_e can be accommodated without a large increase in potential energy from that of the well depth. By contrast, for stiff potentials there is considerable energetic penalty for NN interactions where r does not equal r_e. We shall refer to this as strain energy.

The principles determining the ground-state structure of homogeneous clusters are now well understood. Icosahedral packing optimizes the number of NN interactions. However, the icosahedral motif is also strained. The alternative decahedral packing and close-packing motifs are less strained, but also provide fewer NN contacts. Since the strain penalty is not great for soft potentials, icosahedral packing dominates for small clusters. This is well documented for the Lennard-Jones potential, $(LJ)_N$.[8,26−28,31] In fact, $(LJ)_N$. remains icosahedral for N values well into the thousands, with a few isolated exceptions (such as truncated octahedra, Marks decahedra, the Leary tetrahedron.[28]) By contrast, for fullerene clusters (with stiff potentials) the GM structures adopt less strained geometries for as few as 14 particles.[16,17] The contrast in the growth sequences of soft and stiff potentials has been cataloged extensively.[15,17,22,23,25,28,33]

While considerable work has been done on homogeneous clusters, considerably less effort has been devoted to the details of nonhomogeneous clusters. Binary clusters—containing two types of particle—have received some attention,[18,30−50] but the general level of understanding is still well behind that of the homogeneous clusters, since the parameter space is so large. However, since fullerenes can be generated in a wide variety of sizes, this seems to be a natural area in which mixed clusters with components of different sizes can be investigated experimentally.

Based on the studies of binary clusters, there is some reason to believe that the ratio of "sizes" of the homogeneous components will be an important variable, as we will briefly explain. For convenience, we define the interaction length ratio, $S^I = r_e^{AB}/r_e^{BB}$ (where we have assumed B is the "larger" particle). One important finding has been that a single smaller particle in the central location can relieve the strain felt by the icosahedral cluster. In fact, the choice of $S^I = 0.952$ relieves this strain completely.[36,48]

Most of these studies have focused on (soft) binary LJ (BLJ) systems A_nB_{N-n}. From them, it seems to be clear that the geometry of BLJ clusters is considerably more sensitive to the ratio of interaction lengths of the component species than it is to the ratio of the interaction energies. For S^I close to unity, most compositions are icosahedral, as would be expected for the homogeneous case. However, for values of S^I significantly smaller, strain can be introduced, and geometries not typical of the homogeneous case can be induced.[39] For $n = 0$, the dominant packing motif for most N values is icosahedral. A relatively small number, n, of "impurity" species can be accommodated since they reduce the strain by occupying interior icosahedral sites, preserving the icosahedral geometry. In addition, for values of n close to N, the clusters tend to be icosahedral, with the larger impurity atoms occupying surface sites. However, for near equimolar compositions (n comparable to 50% mole fraction) nonicosahedral structures have been observed.[39]

A recent interesting study of a binary Morse cluster A_nB_{38-n}[46] fixed the energy and length parameters and explicitly varied the stiffness parameter. It was shown that variation of the interaction stiffness parameter alone is capable of driving structural changes in the structure for the 38-mer.

There has been little systematic research in exploring binary mixing for stiff potentials. Since the computational effort required to locate reliable energetic GMs rises steeply as a function of N, it is advantageous to work with smaller clusters. As noted above, structural transitions for clusters with stiff potentials occur for smaller cluster sizes. We therefore expect a richer range of structures for smaller total cluster sizes when looking at binary fullerene clusters than has been the case for BLJ clusters.

To our knowledge, there has only been one study of the cluster geometry of mixed fullerene clusters. Garcia et al.[18] considered the cluster $(C_{60})_n(C_{70})_{N-n}$. ($N = 11-22$) using the Girifalco potential for both pure and mixed interactions.[19,21] They found that all the mixed clusters with $N \leq 13$ were icosahedral. They also noted that all clusters with $N > 21$ were decahedral. Binary clusters that were close to homogeneous ($N > 14$, $n \leq 2$) or ($N > 14$, $n > 12$) tended to be decahedral; equimolar clusters for $13 \leq N \leq 21$ where n approached $N/2$ were found to favor icosahedral packing.

The interaction size ratio, S^I, for the C_{60}/C_{70} system is 0.97, close to unity. This suggests that the binary clusters will tend to look very similar to the homogeneous clusters for the same size; that is, decahedral when $N > 13$. As can be seen from the results of Garcia et al., this is indeed the case. The icosahedral structures were particularly stable when the smaller central species could relieve the strain of an icosahedon, as was the case $(C_{60})_1(C_{70})_{13-1}$ or a double icosahedron such as $(C_{60})_2(C_{70})_{19-2}$. The only geometries reported were icosahedral and decahedral.

In this work, we consider the binary clusters of $(C_{60})_n$-$(C_{84})_{N-n}$ ($N = 6-24$). The interaction size ratio for this system is 0.94. This is a larger deviation from unity than that used in the previous treatment on binary fullerene clusters.[18] It is

TABLE 1: Binding Energies ϵ and Preferred Separations r_e for C_{60} and C_{84} Determined Using Girifalco's Pairwise Additive Potential

	$C_{60}-C_{60}$	$C_{60}-C_{84}$	$C_{84}-C_{84}$
Fullerene radius (Å)	3.55		4.20
r_e (Å)	10.0558	10.7064	11.3568
ϵ/k_B (K)	3218.2	3616.4	4080.0

expected that this should lead to a richer diversity of GM structures than was observed in this earlier work.

In Section II, we outline the potential energy functions used, together with our search techniques. In Section III we present Results and Discussion. Concluding Remarks are in Section IV.

II. Methods

II.A. Potential Energy Functions. Interactions between particles were modeled using Girifalco's pseudoatomic pairwise additive potential derived using the assumption that C-atom density is spherically distributed.[21] Proposed originally for $C_{60}-C_{60}$, this potential has been generalized to account for interactions between larger fullerenes and fullerenes of different sizes.[19] Using this parametrization, the $C_{60}-C_{84}$ equilibrium separation and well depth are within 1% of the Lorentz−Bertholet values based on the parameters of the homogeneous interactions. The equilibrium separations and well depths for this potential are given in Table 1.

II.B. GM Search Method. Unbiased GM searches were carried out using the basin-hopping algorithm,[31] based on the "Monte Carlo-quench" method employed to study protein conformers.[29] Starting from a random configuration of particles in a spherical container, each BH run consisted of 5000 MC move + quench steps subject to a Metropolis acceptance criterion at a fixed temperature of 3500K. The three types of moves employed and their relative abundances were: translations of all particles, 0.8; identity exchange for two nonidentical particles, 0.1; and angular moves for the weakest bound surface particle, 0.1. Translational steps were selected on a flat interval [−1, 1] multiplied by 3 Å. Angular moves were performed by calculating the maximum radius, r_{max}, between the center of mass and every particle, removing the weakest bound particle, and then replacing it with random angular coordinates at distance r_{max} from the center of mass. The angular and identity exchange moves were intended to avoid large energetic barriers separating homotops and to speed transitions between distant regions of the potential energy surface.

GM searches consisting of a maximum of 50 BH runs were performed for all compositions $(C_{60})_n(C_{84})_{N-n}$ up to $N = 24$. For each composition, the 50 overall lowest energy structures from all runs were saved. For small and nearly homogeneous clusters, the majority of the 50 runs located the same putative GM. However, for large approximately equimolar ($n \approx N/2$) clusters, the lowest energy structure was often only found in a single run, and systematic searches were discontinued beyond $N = 24$. Accordingly, we cannot claim with a high degree of confidence that all of the highly mixed structures are GMs, and some could likely be improved. However, unless explicitly noted, all structures discussed are assumed to be putative GMs.

III. Results and Discussion

III.A. Homogeneous Fullerene Clusters. We consider the homogeneous clusters first, since they provide a good overview of many of the concepts required to understand the binary clusters. The $(C_{60})_N$, $N \leq 24$, cluster GMs using the Girifalco potential[21] have been reported in detail elsewhere.[16,17,33] Our findings are in complete agreement with published data for both geometries and energies of the GMs. The GM is icosahedral up to (and including) $N = 13$. However, for $N = 14$, the less strained decahedral geometry is preferred.

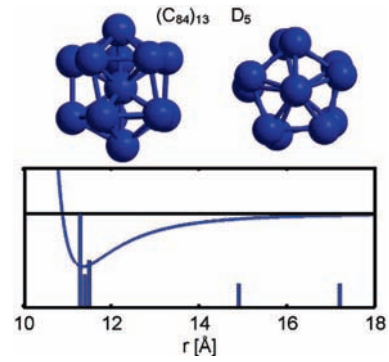

Figure 2. D_5 GM structure of $(C_{84})_{13}$ viewed from two perspectives (upper) and the cluster's radial distribution function plotted with the $C_{84}-C_{84}$ interaction potential on the same horizontal distance scale (lower).

Homogeneous $(C_{84})_N$, $N \leq 24$, clusters have geometries identical to those of the corresponding $(C_{60})_N$ cluster, with the exception of the important case $N = 13$, which we discuss in more detail below. We note in passing that the $N = 6$ GM has octahedral symmetry (as do $(LJ)_6$ and $(C_{60})_6$). As is the case with $(C_{60})_{14}$, for $(C_{84})_{14}$ the packing is decahedral. $(C_{60})_N$ and $(C_{84})_N$ have identical decahedral geometries for $14 \leq N \leq 23$. Both are close-packed for $N = 24$.

The GM structures of 13-mers using a pairwise additive potential are particularly well documented in the literature.[23,25] The GM of the 13-particle Morse cluster, M_{13}, has been investigated as a function of the range parameter. For soft potentials, the icosahedron is preferred, but this preference shifts to a D_{5h} decahedron as the stiffness is increased. These 13-particle icosahedron and decahedral structures both have two five-particle rings which are staggered and eclipsed when viewed along their respective C_5 axes and a torsional twist can interconvert them. The GM structure we report for $(C_{84})_{13}$ lies between these extremes: The five-particle rings in $(C_{84})_{13}$ are almost, but not completely, eclipsed. This removal of the horizontal mirror plane perpendicular to the C_5 axis results in a D_5 structure. We are not aware of previous GM structures of this geometry for 13-mers resulting from pairwise-additive potentials being reported in the literature.

The reason for this geometry can be explained as follows. Since the C_{84} potential is somewhat stiffer ($\rho = 15.1$) than the C_{60} potential ($\rho = 13.6$), its 13-mer might be expected to assume the less strained decahedral motif. However, there is slightly more long-range attraction for the Girifalco potential compared with the fitted Morse potential (see Figure 1a). This results in a slight "twist" of the two five-membered rings to gain a small amount of attractive energy between the two particles diagonal to each other (at $r = \sqrt{2}r_e$) across the exposed {100} faces of the decahedron. This can be seen from Figure 2, where the radial distribution function is shown. For a decahedral cluster, all second NN distances would be $r = \sqrt{2}r_e$ (16.06 Å). The "twist" allows half of these distances to shorten, increasing the energetic stability.

III.B. Binary Clusters with Compositions $(C_{60})_n(C_{84})_{N-n}$, $N \leq 24$. Putative GM structures have been located for cluster sizes $N = 6-24$ and all possible $C_{60}-C_{84}$ compositions. We require a measure of relative stability to understand the structural trends. We use the Laplacian, a sum of the second finite

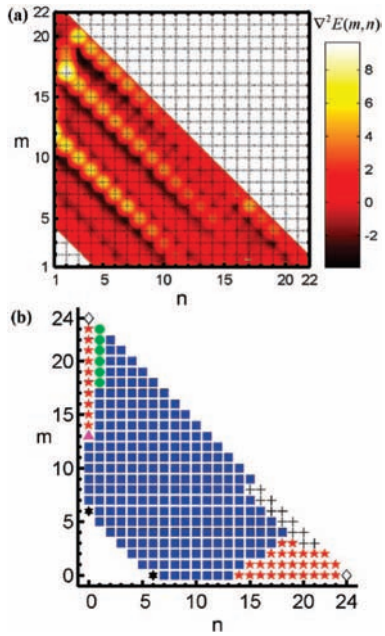

Figure 3. (a) The Laplacian of cluster energy with respect to m and n, the number of C_{84} and C_{60}, respectively. (b) Geometry of the GM. Symbols and respective motifs are: blue square (■), (poly)-icosahedral; black plus (+), polyicosahedral stacked; red star (★), decahedral; black hexagonal star (*), octahedral; green circle (●), Mackay overlayer; white diamond (◊), close packed, and pink triangle (▲), D_5 $(C_{84})_{13}$.

differences with respect to $m = N - n$ and n, the number of C_{84} and C_{60}, respectively. This is expressed as

$$\nabla^2 E_{m,n} = \Delta_2 E_m + \Delta_2 E_n$$
$$= (E_{m+1,n} + E_{m-1,n} + E_{m,n+1} + E_{m,n-1}) - 4E_{m,n} \quad (2)$$

Figure 3a shows the results. Varying $N = m + n$ leads to qualitative changes in the Laplacian. However, for constant N, variation in the composition, n, leads to more subtle changes.

Structures for all GMs were determined by visual inspection and a composition phase diagram was constructed (Figure 3b). We note that a majority of C_{60}-C_{84} clusters are (poly)icosahedral. "Almost" pure clusters tend to be decahedral, with the region of stability for this being greater for compositions where C_{84} is the majority component. In the following section, we further detail these features of the phase diagram.

III.B.I. GM Structures. Polyicosahedral packing—in which interior particles have icosahedral coordination shells—is the most commonly observed motif for most of the binary clusters in this study. This is in contrast to the previously reported work on $C_{60}-C_{70}$ clusters, where a smaller fraction of compositions had this structure.[18] Nonpolyicosahedral structures were only found for C_{60}-rich and C_{84}-rich compositions; that is, almost-homogeneous clusters.

Cluster sizes $N = 13$, $N = 19$ and 23 show particular relative stability in Figure 3. These are N values which correspond to closed shell polyicosahedral structures. The most stable compositions at these sizes were the $(C_{60})_1(C_{84})_{12}$, $(C_{60})_2(C_{84})_{17}$, and $(C_{60})_3(C_{84})_{20}$, and can be viewed as a monomer, dimer and trimer of C_{60}, respectively, where each C_{60} has its remaining icosahedral NN shell completed with C_{84}. These are shown in Figure 4a, b, and c, respectively. Each icosahedral subunit of these clusters is equivalent to the $(C_{60})_1(C_{84})_{12}$ GM with one or two external C_{84} changed to C_{60}. The RDFs confirm that the NN interactions are all tightly distributed about their preferred separations.

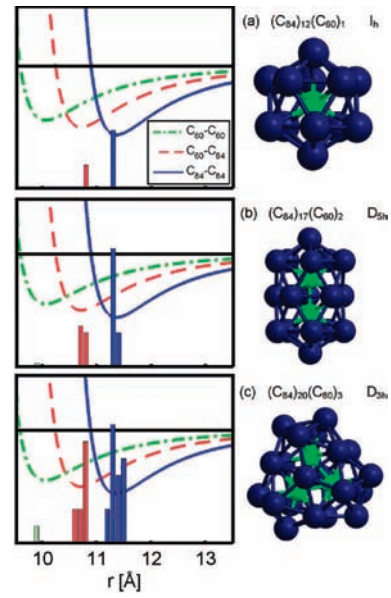

Figure 4. Polyicosahedral GM structures with C_{84} and C_{60} represented as blue and green balls, respectively. The relevant portions of their respective radial distribution functions are shown superimposed on the pair potentials.

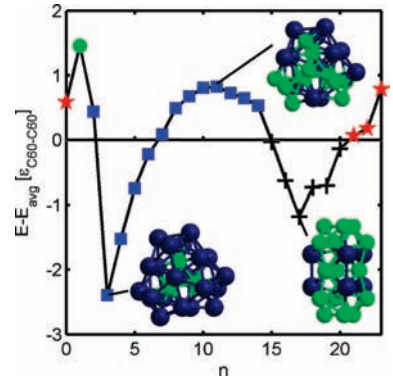

Figure 5. Difference between GM energy and mean energy for binary fullerene clusters with $N = 23$ as a function of n. The symbols are the same in Figure 3. Also shown are the GM structures for $n = 3$, 11, and 17.

Next we consider the changes in GM structure as cluster composition is varied but N is held constant. We highlight the $N = 23$ case. Figure 5 compares the GM energies and indicates the GM structure as the number of C_{60} fullerenes, n, increases. (For simplicity, n alone will be used to denote clusters in this series.) The end points $n = 0$ and $n = 23$ correspond to $(C_{84})_{23}$ and $(C_{60})_{23}$, which have identical decahedral structures. However an asymmetry in energies and structure is apparent as n is varied. These transitions are described below.

First, at $n = 1$ a single impurity particle changes the structure from decahedral to an incomplete $N = 55$ Mackay icosahedron. (The series of Mackay structures is discussed in more detail later.) Polyicosahedral structures dominate for $n = 2$ to 14.

The potential energy sharply drops to its minimum for the highly stable $n = 3$ structure (Figure 4c) described previously. Successive GMs maintain the same compact polyicosahedral structure as n is increased; however, the relative energy quickly

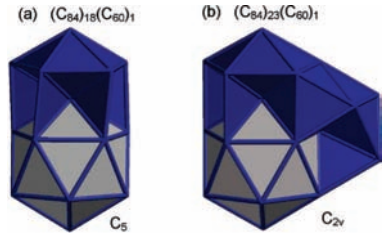

Figure 6. GM structures with partial Mackay overlayers. A C_{84} is located at each vertex. Gray panels emphasizes the $(C_{60})_1(C_{84})_{12}$ core and blue panels highlight the Mackay overlayer.

rises due to the strain penalties associated with icosahedral packing. The strained, nearly equimolar $n = 11$ GM is shown in Figure 5.

At $n = 15$ through $n = 20$, clusters adopt a less strained polyicosahedral motif in which two "stacked" icosahedra share only a common triangular face and a C_3 axis. This structural change is evident in the energetic trend. The high symmetry/low energy structure $n = 17$ shown in Figure 5 demonstrates a second, much less common, way that polyicosahedral packing is stabilized in binary clusters. This structure is stabilized because the six large, external C_{84} form a triangular prism to join the two icosahedral units. (We note that the Dzugutov potential[50]—which has a positive potential energy at $-2r_e$ to disfavor octahedral interstices and promote polytetrahedral structures—has the same GM for $N = 23$.[24]) However, this is an unusual structure for clusters with realistic pairwise additive potentials.

Finally, for $n = 21$ through 23, the unstrained decahedral packing of the homogeneous cluster is restored. We note that the N-n C_{84} in $n = 21$ and 22 occupy external surface sites and do not induce structural changes.

For the series of compositions $(C_{60})_1(C_{84})_{N-1}$, a single C_{60} impurity changes the GM structure from decahedral to Mackay icosahedral (Figure 3b).[48] Structurally, only the central C_{60} particle has icosahedral coordination to its 12 NN while all C_{84} have decahedral local packing. The columnar $(C_{60})_1(C_{84})_{17}$ cluster (Figure 6a) clearly demonstrates this coexistence of localized icosahedral and decahedral packing while $(C_{60})_1(C_{84})_{23}$ (Figure 6b) shows further Mackay overlayer growth.

The stability of the Mackay structures is attributed to both the $(C_{60})_1(C_{84})_{12}$ core's stability and the tendency of homogeneous C_{84} to avoid strained icosahedral packing. It also suggests that rich competition likely exists between Mackay, decahedral, and close packed morphologies beyond the $N = 24$ limit of this study.

IV. Concluding Remarks

We have obtained the putative global minimum geometries for binary mixed clusters of C_{84} and C_{60} fullerenes using the stiff Girifalco pairwise additive potential up to a total cluster size of $N = 24$. We report the putative global minimum geometries of homogeneous $(C_{84})_N$ clusters. In the size range reported, they are identical to those reported for the homogeneous $(C_{60})_N$ clusters: For $N < 12$ most are icosahedral; for N between 14 and 23 they are decahedral, with $N = 24$ being close packed. One exception to this similarity is the $N = 13$ case. This cluster has a D_5 geometry. To the best of our knowledge, this is the first reported homogeneous 13-particle cluster whose potential is pairwise additive that has this structure.

Because the fullerene−fullerene interaction potential is stiff, a variety of different morphologies in the cluster geometry is available for a relatively small cluster size, N. For the binary clusters studied, polyicosahedral structures are observed for a wide range of cluster sizes and compositions. The favorable interaction length ratio, S^I reduces the strain associated with these structures and produces a number of motifs not seen in homogeneous fullerene clusters. An asymmetry is noted in the structural transitions between the polyicosahedral mixed compositions and the primarily decahedral homogeneous clusters. For example, Mackay-icosahedron based GMs were found for clusters $(C_{60})_1$ $(C_{84})_{N-1}$, $N > 18$ containing only a single C_{60}. Additionally, for $N = 23$ and $N = 24$, we observe a reduced strain "stacked" polyicosahedral motif for limited compositions separating the compact polyicosahedral and decahedral stability regions. These latter two types of structure were not observed in the only previous study of mixed fullerene clusters.[18]

For fullerenes, the size ratio of the component species can be readily varied. Our results suggest that further studies of larger clusters and perhaps other fullerene species could be fruitful in exploring how noncovalent interactions between fullerenes can control self-assembly of supramolecular structures containing fullerene derivatives.

Acknowledgment. This work was funded by the Center for High-Rate Nanomanufacturing. (National Science Foundation Award # NSF-0425826.)

References and Notes

(1) Kroto, H. W.; Heath, J. R.; O'Brien, S. C.; Curl, R. F.; Smalley, R. E. *Nature* **1985**, *318*, 162–163.
(2) Bonifazi, D.; Enger, O.; Diederich, F. *Chem. Soc. Rev.* **2007**, *36*, 390–414.
(3) Shirai, Y.; Cheng, L.; Chen, B.; Tour, J. *J. Am. Chem. Soc.* **2006**, *128*, 13479–13489.
(4) Guldi, D. M. In *Nanoparticles and Nanostructured Films*; Wiley-VCH: Weinheim, 1998; pp 119−143.
(5) Maruccio, G.; Cingolani, R.; Rinaldi, R. *J. Mater. Chem.* **2004**, *14*, 542–554.
(6) Zhang, E.; Wang, C. *Current Opinion Coll. Interface Sci.* **2007**, . in press.
(7) Georgakilas, V.; Pellarini, F.; Prato, M.; Guldi, D. M.; Melle-Franco, M.; Zerbetto, F. *Proc. Natl. Acad. Sci. U.S.A.* **2002**, *99*, 5075–5080.
(8) Hahn, U.; Cardinali, F.; Nierengarten, J. *New J. Chem.* **2007**, *31*, 1128–1138.
(9) Wang, Y.; Alcamí, M.; Martín, F. *ChemPhysChem.* **2008**, *9*, 1030–1035.
(10) Lehn, J. *Angew. Chem., Int. Ed.* **1990**, *29*, 1304–1319.
(11) Wales, D. J. *Energy Landscapes*; Cambridge University Press: Cambridge, 2004.
(12) Dykstra, C. E.; Lisy, J. M. *J. Mol. Structure THEOCHEM.* **2000**, *500*, 375–390.
(13) Ferrando, R.; Jellinek, J.; Johnston, R. L. *Chem. Rev.* **2008**, *108*, 845.
(14) Hartke, B. *Angew. Chem., Int. Ed.* **2002**, *41*, 1468–1487.
(15) Cai, W.; Feng, Y.; Shao, X.; Pan, Z. *Chem. Phys. Lett.* **2002**, *359*, 27–34.
(16) Doye, J. P. K.; Wales, D. J. *Chem. Phys. Lett.* **1996**, *262*, 167–174.
(17) Doye, J. P. K.; Wales, D. J.; Branz, W.; Calvo, F. *Phys. Rev. B.* **2001**, *64*, 235409.
(18) Garcia, R.; Rey, C.; Gallego, L. J. *J. Chem. Phys.* **1998**, *108*, 9199–9201.
(19) Kniaz, K.; Fischer, J. E.; Girifalco, L. A.; McGhie, A. R.; Strongin, R. M.; Smith, A. B. *Solid State Commun.* **1995**, *96*, 739–743.
(20) Zhang, W.; Liu, L.; Zhuang, J.; Li, Y. *Phys. Rev. B.* **2000**, *62*, 8276.
(21) Girifalco, L. A. *J. Phys. Chem.* **1992**, *96*, 858–861.
(22) Doye, J. P. K.; Wales, D. J. *Faraday Trans.* **1997**, *93*, 4233–4243.
(23) Doye, J. P. K.; Wales, D. J.; Berry, R. S. *J. Chem. Phys.* **1995**, *103*, 4234–4249.
(24) Doye, J. P. K.; Wales, D. J.; Simdyankin, S. I. *Faraday Disc.* **2001**, *118*, 159–170.
(25) Miller, M. A.; Doye, J. P. K.; Wales, D. J. *J. Chem. Phys.* **1999**, *110*, 328–334.
(26) Northby, J. A. *J. Chem. Phys.* **1987**, *87*, 6166–6177.
(27) Pullan, W. *J. Comput. Chem.* **2005**, *26*, 899–906.

(28) Xiang, C.; Cai, S. *J. Phys. Chem. A.* **2004**, *108*, 9516–9520.
(29) Li, Z.; Scheraga, H. A. *Proc. Natl. Acad. Sci. U.S.A.* **1987**, *84*, 6611–6615.
(30) Munro, L. J.; Tharrington, A.; Jordan, K. D. *Comput. Phys. Commun.* **2002**, *145*, 1–23.
(31) Wales, D. J.; Doye, J. P. *J. Phys. Chem. A.* **1997**, *101*, 5111–5116.
(32) Pullan, W. J. *J. Comput. Chem.* **1997**, *18*, 1096–1111.
(33) Calvo, F.; Yurtsever, E. *Phys. Rev. B.* **2004**, *70*, 045423.
(34) Cozzini, S.; Ronchetti, M. *Phys. Rev. B.* **1996**, *53*, 12040.
(35) Doye, J. P. K.; Meyer, L. *Phys. Rev. Lett.* **2005**, *95*, 063401–4.
(36) Ferrando, R.; Fortunelli, A.; Johnston, R. L. *Phys. Chem. Chem. Phys.* **2008**, *10*, 640–649.
(37) Frantz, D. D. *J. Chem. Phys.* **1996**, *105*, 10030–10049.
(38) Frantz, D. D. *J. Chem. Phys.* **1997**, *107*, 1992–2011.
(39) Cleary, S. M.; Mayne, H. R. *Chem. Phys. Lett.* **2006**, *418*, 79–83.
(40) Iwamatsu, M. *Mater. Sci. Eng.: A* **2007**, *449−451*, 975–978.
(41) Iwamatsu, M.; Lai, S. *J. Non-Cryst. Solids* **2007**, *353*, 3698–3703.
(42) Sabo, D.; Doll, J. D.; Freeman, D. L. *J. Chem. Phys.* **2003**, *118*, 7321–7328.
(43) Sabo, D.; Predescu, C.; Doll, J. D.; Freeman, D. L. *J. Chem. Phys.* **2004**, *121*, 856–867.
(44) Sabo, D.; Doll, J. D.; Freeman, D. L. *J. Chem. Phys.* **2004**, *121*, 847–855.
(45) Parodi, D.; Ferrando, R. *Phys. Lett. A.* **2007**, *367*, 215–219.
(46) Rey, C.; Gallego, L. J.; Alonso, J. A. *Phys. Rev. B.* **1994**, *49*, 8491.
(47) Mackay, A. L. *Acta Crystallogr.* **1962**, *15*, 916.
(48) Kob, W.; Andersen, H. C. *Phys. Rev. Lett.* **1994**, *73*, 1376.
(49) Doye, J. P. K.; Louis, A. A.; Lin, I.; Allen, L. R.; Noya, E. G.; Wilber, A. W.; Kok, H. C.; Lyus, R. *Phys. Chem. Chem. Phys.* **2007**, *9*, 2197–2205.
(50) Dzugutov, M. *Phys. Rev. A.* **1992**, *46*, R2984.

JP811290H